Article

Chinese Science Bulletin

SPECIAL ISSUE: Graphene

August 2012 Vol.57 No.23: 3030–3035
doi: 10.1007/s11434-012-5286-9

Fabrication of carbon nanotube/graphene core/shell nanostructures on SiO_2 substrates using organic solvents: A molecular dynamics study

LING CuiCui[1,2,3], XUE QingZhong[1,2,3*] & JING NuanNuan[1]

[1] *College of Science, China University of Petroleum, Qingdao 266580, China;*
[2] *Key Laboratory of New Energy Physics & Materials Science in Universities of Shandong, China University of Petroleum, Qingdao 266580, China;*
[3] *State Key Laboratory of Heavy Oil Processing, China University of Petroleum, Qingdao 266580, China*

Received November 12, 2011; accepted February 2, 2012

Using molecular mechanics and molecular dynamics simulations, we demonstrate that it is difficult to fabricate single-walled carbon nanotube (SWNT)/carbon nanoscroll (CNS) core/shell nanostructures on solid substrates because of the strong interaction between the graphene (GN) and the substrate. We propose an effective way to reduce the interaction between the GN and the substrate; SWNT/CNS core/shell nanostructures can be fabricated easily on SiO_2 substrates by exploiting the volatilization of organic solvents, and inducement with SWNTs. These SWNT/CNS core/shell nanostructures on SiO_2 substrates have the potential to be applied in telecom network transmission, or as electronic components in apparatuses such as microcircuit interconnects, nanoelectronics devices, heterojunctions, or sensors.

core/shell nanostructures, nanoscrolls, substrates, organic solvents, heterojunctions

Citation: Ling C C, Xue Q Z, Jing N N. Fabrication of carbon nanotube/graphene core/shell nanostructures on SiO_2 substrates using organic solvents: A molecular dynamics study. Chin Sci Bull, 2012, 57: 3030–3035, doi: 10.1007/s11434-012-5286-9

Carbon nanotubes (CNTs) and graphene (GN) have attracted tremendous interest because of their unique properties and their promise for applications, which result from their ideal 1 and 2D structures [1−4]. The properties of CNTs have been investigated in great detail in recent years, and researches into GN are rapidly catching up with that of CNTs. Recently, carbon nanoscrolls (CNSs) have attracted much attention; these structures are composed of a continuous GN sheet rolled up in a spiral form. CNSs have a structure similar to that of multi-walled carbon nanotubes (MWNT), but the interlayer spacing and core size of CNSs can be varied; this is not true of MWNTs. CNSs can therefore be tuned to better contain and encapsulate functional molecules or nanomaterials into the interlayer spaces of the scrolls, and are considered as promising materials for hydrogen storage, supercapcacitors, water channels, nano-oscillators, and nano-actuators.

Both fundamental interest and the promise of technical applications for CNS materials have motivated many researchers [5−8]. Previously, a number of methods for the synthesis of CNSs have been proposed, including the arc-discharge method [9], the high-energy ball milling of graphite [10], and the chemical route [11−13]. However, the disadvantages of these methods in the fabrication, isolation, and device integration of high-quality CNSs mean that further investigation of these techniques is not desirable. Recently, many theoretical analysis and molecular dynamics (MD) simulations have shown that suspended carbon nanoribbons or GN can spontaneously form CNSs in vacuum [14,15]. However, the fabrication of CNSs on solid substrates is more desirable; solid substrates can meet the demands of practical technology applications. It is known that

*Corresponding author (email: xueqingzhong@tsinghua.org.cn)

a strong van der Waals interaction exists between GN and solid substrates [16,17], which hinders the formation of CNS structures on solid substrates. To reduce the influence of the van der Waals interaction between the GN and the solid substrates, experimental attempts have been made to produce CNSs from GN on solid substrates, using compressing force [18], electrostatic fields [8,19], and surface gas adsorption [20]. These methods are effective approaches for producing large numbers of CNSs on solid substrates; however, they do not allow control over the diameter and chirality of CNSs.

In this paper, we proposed a simple method for the synthesis of single-walled CNT (SWNT)/GN core/shell nanostructures on solid substrates, using the volatilization of organic solvents, and SWNT-inducement. Using this method, we were able to fabricate a large number of CNSs on solid substrates, via a reduction in the van der Waals interaction between the GN and solid substrate. In addition, the diameter and chirality of the CNSs could be controlled using this method.

1 Experimental

1.1 Computational method

Molecular mechanics (MM) and MD simulations were carried out using a commercial software package called Materials Studio (MS), developed by Accelrys Software Inc of San Diego, CA. All MD simulations were performed in the NVT ensemble, and a fixed time-step size of 1 fs was used in all cases. The Andersen thermostat method was employed to maintain the system at a temperature of 600 K, and the interactions were determined within a cutoff distance of 9.5 Å. MM simulations were performed to find a thermally stable morphology, and to achieve a conformation with a minimum potential energy for the SWNTs and GN.

The condensed phase optimization molecular potentials for atomistic simulation studies (COMPASS) module in the Materials Studio software was used to conduct force-field computations. The COMPASS is a parameterized, tested, and validated first *ab initio* force field [21,22] that enables the accurate prediction of various gas-phase and condensed-phase properties of most common organic and inorganic materials [23–25].

1.2 Force field

The application of quantum mechanical techniques can accurately simulate a system of interacting particles, but such techniques often use too much time, and are typically only feasible in systems containing up to a few hundred interacting particles. The main goal of simulations of systems containing a large number of particles is generally to obtain the systems' bulk properties, which are primarily controlled by the location of the atomic nuclei; in this case, the knowledge of the electronic structure provided by quantum mechanical techniques is not critical. We can therefore gain a good insight into the behavior of a system if a reasonable, physically based approximation of the potential (force field) can be obtained; this can be used to generate a set of system configurations that are statistically consistent with a fully quantum mechanical description. As stated above, a crucial point in the atomistic simulations of multi-particle systems is the choice of the force fields, a brief overview of which is given in this section.

In general, the total potential energy of a molecular system includes the following terms [26]:

$$E_{\text{total}} = E_{\text{valence}} + E_{\text{cross-term}} + E_{\text{non-bond}}, \tag{1}$$

$$E_{\text{valence}} = E_{\text{bond}} + E_{\text{angle}} + E_{\text{torsion}} + E_{\text{oop}} + E_{\text{UB}}, \tag{2}$$

$$\begin{aligned} E_{\text{cross-term}} = {} & E_{\text{bond-bond}} + E_{\text{angle-angle}} + E_{\text{bond-angle}} + E_{\text{end-bond-torsion}} \\ & + E_{\text{middle-bond-torsion}} + E_{\text{angle-torsion}} + E_{\text{angle-angle-torsion}}, \end{aligned} \tag{3}$$

$$E_{\text{non-bond}} = E_{\text{vdW}} + E_{\text{Coulomb}} + E_{\text{H-bond}}. \tag{4}$$

The valence energy, E_{valence}, generally includes a bond stretching term, E_{bond}; a two-bond angle term, E_{angle}; a dihedral bond-torsion term, E_{torsion}; an inversion (or an out-of-plane interaction) term, E_{oop}; and a Urey-Bradlay term (representing interactions between two atoms bonded to a common atom), E_{UB}. The cross-term interacting energy, $E_{\text{cross-term}}$, generally includes stretch-stretch interactions between two adjacent bonds, $E_{\text{bond-bond}}$; bend-bend interactions between two valence angles associated with a common vertex atom, $E_{\text{angle-angle}}$; stretch-bend interactions between a two-bond angle and one of its bonds, $E_{\text{bond-angle}}$; stretch-torsion interactions between a dihedral angle and one of its end bonds, $E_{\text{end-bond-torsion}}$; stretch-torsion interactions between a dihedral angle and its middle bond, $E_{\text{middle-bond-torsion}}$; bend-torsion interactions between a dihedral angle and one of its valence angles, $E_{\text{angle-torsion}}$, and bend-bend-torsion interactions between a dihedral angle and its two valence angles, $E_{\text{angle-angle-torsion}}$. The non-bond interaction term, $E_{\text{non-bond}}$, accounts for the interactions between non-bonded atoms, and includes the van der Waals energy, E_{vdW}, the Coulomb electrostatic energy, E_{Coulomb}, and the hydrogen-bond energy, $E_{\text{H-bond}}$.

The dompass force field uses different expressions for various components of the potential energy, as follows [23,24]:

$$\begin{aligned} E_{\text{valence}} = {} & \sum_b \left[K_2(b-b_0)^2 + K_3(b-b_0)^3 + K_4(b-b_0)^4 \right] \\ & + \sum_\theta \left[H_2(\theta-\theta_0)^2 + H_3(\theta-\theta_0)^3 + H_4(\theta-\theta_0)^4 \right] \\ & + \sum_\varphi \left[V_1\left[1-\cos(\varphi-\varphi_1^0)\right] + V_2\left[1-\cos(2\varphi-\varphi_2^0)\right] \right. \\ & \left. + V_3\left[1-\cos(3\varphi-\varphi_3^0)\right] \right] + \sum_x K_x \chi^2 + E_{\text{UB}}. \end{aligned} \tag{5}$$

$$
\begin{aligned}
E_{\text{cross-term}} = & \sum_{b}\sum_{b'} F_{bb'}(b-b_0)(b'-b_0') \\
& + \sum_{\theta}\sum_{\theta'} F_{\theta\theta'}(\theta-\theta_0)(\theta'-\theta_0') \\
& + \sum_{b}\sum_{\theta} F_{b\theta}(b-b_0)(\theta-\theta_0) \\
& + \sum_{b}\sum_{\varphi} F_{b\varphi}(b-b_0) \\
& \times[V_1\cos\varphi + V_2\cos 2\varphi + V_3\cos 3\varphi] \\
& + \sum_{b'}\sum_{\varphi} F_{b'\varphi}(b'-b_0')(b'-b_0') \\
& \times[F_1\cos\varphi + F_2\cos 2\varphi + F_3\cos 3\varphi] \\
& + \sum_{\theta}\sum_{\varphi} F_{\theta\varphi}(\theta-\theta_0) \\
& \times[V_1\cos\varphi + V_2\cos 2\varphi + V_3\cos 3\varphi] \\
& + \sum_{\varphi}\sum_{\theta}\sum_{\theta'} K_{\varphi\theta\theta'}\cos\varphi(\theta-\theta_0)\times(\theta'-\theta_0'). \qquad (6)
\end{aligned}
$$

$$
E_{\text{non-bond}} = \sum_{i>j}\left[\frac{A_{ij}}{r_{ij}^9} - \frac{B_{ij}}{r_{ij}^6}\right] + \sum_{i>j}\frac{q_i q_j}{\varepsilon r_{ij}} + E_{\text{H-bond}}, \qquad (7)
$$

where q is the atomic charge, ε is the dielectric constant, and r_{ij} is the i-j atomic separation distance. b and b' are the lengths of two adjacent bonds, θ is the two-bond angle, φ is the dihedral torsion angle, and χ is the out-of-plane angle. b_0, $k_i(i=2-4)$, θ_0, $H_i(i=2-4)$, $\varphi_i^0(i=1-3)$, $V_i(i=1-3)$, $F_{bb'}$, b_0', $F_{\theta\theta'}$, θ_0', $F_{b\theta}$, $F_{b\varphi}$, $F_{b'\theta}$, $F_i(i=1-3)$, $F_{\theta\varphi}$, $K_{\varphi\theta\theta'}$, A_{ij}, and B_{ij} were fitted from quantum mechanics calculations, and were implemented into the Discover Module of Materials Studio, the commercial atomic simulation program used in this work.

1.3 Molecular model

It has been demonstrated that the metallicity of solid substrates has a great effect on the interaction energy between SWNTs and substrates [27]. For comparison, we chose four representative solids with different metallicities as substrates; namely, Fe, graphite, Si, and SiO_2.

Table 1 gives information for all of substrates used to support the SWNT/GN structures (Fe, graphite, Si, and SiO_2). All of the substrates were built with a similar size and thickness. The SWNTs and GN were built using MS, and the unsaturated boundary effects of the SWNTs were avoided by adding hydrogen atoms. Each C–C bond length was 1.42 Å, and the C–H bond length was 1.14 Å. The hydrogen atoms had a charge of +0.1268 e, the carbon atoms connecting hydrogen atoms had a charge of –0.1268 e; thus, neutrally charged SWNTs (8, 8) (31 Å width) and armchair GN (19 Å width) were constructed.

Table 1 Information for Fe, graphite, Si, and SiO_2 substrates

Substrate	Thickness (Å)	Lattice parameter	Number of atoms
Fe (001)	14.33	42.99 Å×131.85 Å×95.42 Å	8642
Graphite (001)	13.60	41.82 Å×127.83 Å×93.60 Å	9904
Si (001)	13.58	42.24 Å×126.72 Å×96.42 Å	5425
SiO_2 (001)	14.09	42.79 Å×128.37 Å×98.14 Å	6676

2 Results and discussion

2.1 Dynamic behaviors of the SWNT/GN on substrates

MD simulations were conducted to investigate the dynamic behaviors of the SWNT/GN structures on Fe, graphite, Si, and SiO_2 substrates. As shown in Figure 1, to limit the inner core size of the CNS during linear motion, a SWNT was added to the system to induce the initial formation of the CNS. The simulation was run for 400 or 1000 ps until the whole system reached equilibrium. Figure 1 shows the final SWNT/GN configurations on Fe, graphite, Si, and SiO_2. On the Fe substrate, the SWNT did not induce the GN to roll up. On the contrary, the SWNT fully collapsed, and rapidly transformed into linked double graphitic layers parallel to the plane, like a ribbon on the GN surface. Similar dynamic SWNT collapse behavior had been reported in previous studies [27]. On the graphite and Si substrates, the SWNT did not collapse on the GN surface, but also did not induce the GN to form CNSs. These results suggested that the initiative force between the SWNT and the GN was smaller than the strong resistant force between the GN and the Fe (graphite, or Si) substrate. On the SiO_2 substrate, we observed that the GN could wrap the whole SWNT and form one-cycle CNSs. When the SWNT was placed along the left edge of a GN sheet supported by the SiO_2 substrate, the SWNT-GN interaction energy，which served as the driving force，was strong enough to overcome the GN-SiO_2 interaction energy representing the resistant force. The GN atoms close to the SWNT therefore moved rapidly towards

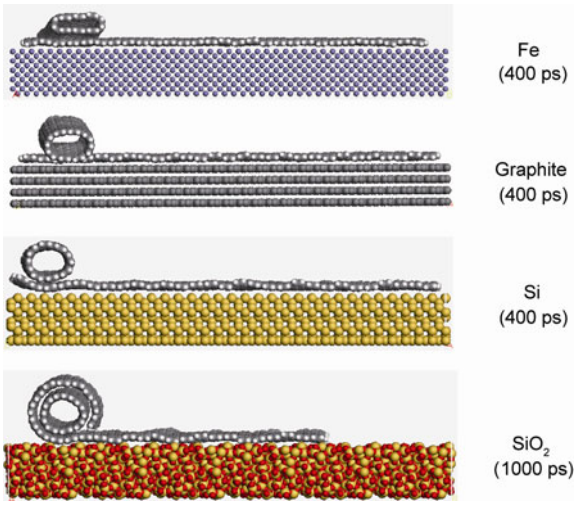

Figure 1 Final configurations of SWNT/GN on Fe, graphite, Si, and SiO_2 substrates.

the SWNT, and attached onto the SWNT surface. Strain was present in the curly GN. When the GN was rolled up into a CNS, there was an interaction force between the GN-GN interlayers; this became the driving force. Because the GN-GN interaction force was smaller than the GN-SiO_2 interaction force and the GN strain, there was a local energy barrier hindering further rolling of the GN [19]. Therefore, only one-cycle CNSs could be fabricated from GN on the SiO_2 substrate. These simulations showed that it was impracticable to form multi-walled CNSs from GN on SiO_2 substrates when only SWNT-inducement was employed.

2.2 Interaction energy between GN and substrates

The interaction energy, reflecting the adhesion between GN and Fe, graphite, Si or SiO_2 substrates, is defined as

$$E_{\text{interaction}} = E_{\text{total}} - (E_{\text{GN}} + E_{\text{substrate}}), \quad (8)$$

where E_{total} is the energy of the system including the GN and the substrate, E_{GN} is the energy of the GN in the absence of a substrate, and $E_{\text{substrate}}$ is the energy of the substrate in the absence of GN. To study the influence of the interactions between GN and the substrate on the formation of CNS in detail, we calculated the interaction energies between the GN and the substrates, as shown in Figure 2. From Figure 2, we can observe that the interaction energies between the GN and the substrates show a decreasing trend, in the sequence $E_{\text{interaction-Fe}} > E_{\text{interaction-graphite}} > E_{\text{interaction-Si}} > E_{\text{interaction-SiO}_2}$. It was found that the interaction energy between the GN and the substrate decreased with decreasing metallicity of the substrate. In addition, the larger the interaction energy between the GN and the substrate was, the smaller the ability of the SWNT to induce GN to scroll on the substrate was, as shown in Figure 1.

2.3 Fabrication of SWNT/GN nanoscrolls core/shell composite nanostructures on substrates

To reduce the influence of the interaction between GN and substrates, Xie et al. [20] fabricated CNSs on a SiO_2 substrate, employing the physical principle of the bending of thin films driven by surface gas adsorption-induced stress. In their experiments, GN was extracted by the mechanical exfoliation of natural graphite on a degenerately doped Si wafer covered with 285 nm of SiO_2. A droplet of isopropyl alcohol (IPA) solution was then placed on the GN monolayer, and one of its straight edges started to roll into a CNS. This occurred because of the surface strain in the upper surface of the GN in the IPA solution, and the volatilization of the IPA molecules; in this process, IPA molecules entered into the space between the GN and the substrate, promoting the formation of CNSs. Xie et al. also discussed another interest-worthy issue regarding the creation of CNSs on substrates; specifically, how to control the diameter and chirality of CNSs, abilities that would facilitate the application of CNSs as microcircuit interconnects. Recently, researchers [28,29] were able to make graphene oxide (GO) nanosheets disperse on many organic solvent surfaces, forming a monolayer of scattering GO sheets using the Langmuir-Blodgett (LB) technique. Liquid surfaces are an ideal platform for graphene, since the soft, fluidic "substrate" perfectly accommodates the flexible sheets, and allows for their free movement on the substrate [28]. On the basis of this research, Gao et al. [18] investigated the highly efficient fabrication of nanoscrolls on liquid surfaces from functionalized graphene oxide, using the LB method. However, it is impossible to control the diameter and chirality of CNSs using these methods. In this work, we demonstrate a novel method for fabricating SWNT/GN nanoscroll core/shell composite nanostructures on substrates, using SWNT-inducement and the volatilization of organic solvents. There have been several reports of core/shell structures with excellent properties, including the electronic property [30] and photoelectronic property [31]. These properties make the core/shell structures promising materials candidates of applications such as nanoelectronic devices or integrated circuits.

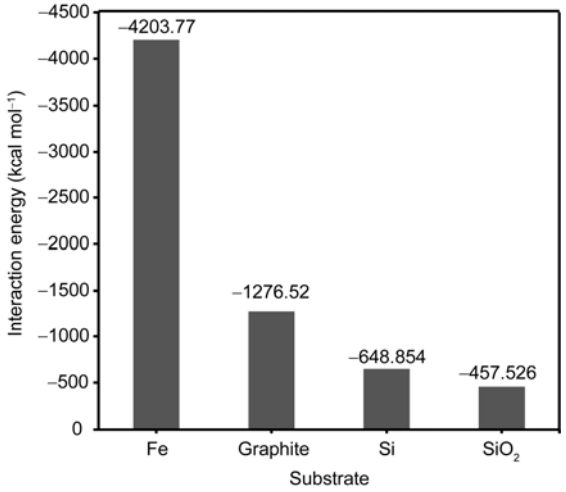

Figure 2 Interaction energies between GN and Fe, graphite, Si, and SiO_2 substrates. 1 cal=4.18 J.

On the basis of the above analysis, as shown in Figure 3, to eliminate the strong interaction between the GN and substrates, we used SWNT-inducement and the volatilization of organic solvents to facilitate the formation of CNSs on substrates. The surface density of graphene is 0.77 mg m^{-2}, which is lower than that of organic solvents. Moreover, the intrinsic SWNT and GN cannot be directly dispersed in organic solvents. We were therefore able to build a model in which the SiO_2 substrates were placed under the organic solvents, and the SWNT/GN structure was laid on the surface of the organic solvents. This model is shown in Figure 3(a). Here, the density of organic solvent *n*-pentane (C_5H_{12}) liquid is 0.613 g cc^{-1} (300 K). The thickness of liquid layer was 18 Å, which was larger than the cutoff distance of 9.5 Å.

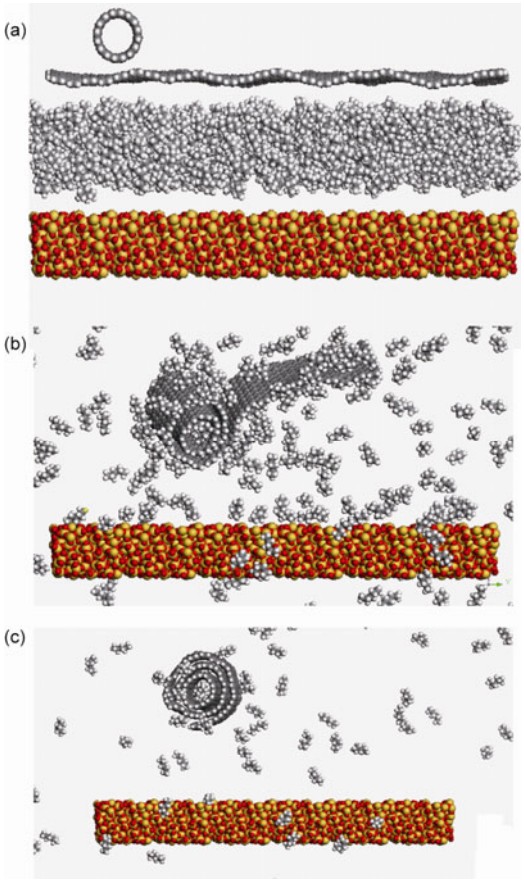

Figure 3 Fabrication of CNSs, achieved using organic solvents between the GN and substrates, and the SWNT-inducement.

The simulations were conducted using MD with a canonical NVT ensemble, and were run for 4000 ps at a temperature of 600 K; this was done to reduce the simulation time and to quickly simulate the volatilization and expansion processes of the gas [32]. It is well known that C_5H_{12} liquid can be volatile at room temperature. After a while, the C_5H_{12} liquid volatilized into a gas that supported the GN, and the SWNT then induced the GN to roll into a CNS. As shown in Figure 3(c), if the simulation time had continued to increase, the SWNT/CNS core/shell composite nanostructures would have fallen to the SiO_2 substrate. Here, the substrates could be random. In contrast with Xie et al. [20] and Gao et al.'s [18] research, our proposed method allowed control over the process of CNS fabrication. In addition, this method allowed us to regulate the core size, and CNS chirality and diameter, via SWNT-inducement; metal/semiconductor type, metal/metal type, or semiconductor/semiconductor type junctions could be created on SiO_2 substrates.

3 Conclusions

In summary, MM and MD simulations were conducted to investigate the scrolling of GN, which was achieved via the use of SWNT-inducement on different solid substrates. The results showed that the GN on the substrates could not form multi-walled CNSs composites when only SWNT-inducement was employed, because of the strong adsorption of the GN on the substrates. The MD simulations showed that an effective way to reduce the interaction between the GN and substrates was to employ an organic solvent between the GN and substrate; using this technique, SWNT/CNS core/shell nanostructures could be easily fabricated on SiO_2 substrates using the volatilization of organic solvents. Moreover, this method should allow a potentially controllable yield of a series of new types of carbon/carbon core/shell composite nanostructures to be created, using the regulation of the CNS chirality and the SWNT chirality. For example, semiconductor/semiconductor and semiconductor/metal types of SWNT/GN core/shell composites could be created on SiO_2 substrates; these materials would have the potential to facilitate applications in microcircuit interconnects, electronics devices, heterojunctions, sensors, thermoelectrics, and optoelectronic devices.

This work was supported by the National Natural Science Foundation of China (*10974258*), *the Program for New Century Excellent Talents in University* (*NCET-08-0844*), *and the Natural Science Foundation of Shandong Province* (*ZR2010AL009*).

1 Huang J Q, Zhang Q, Zhao M Q, et al. A review of the large-scale production of carbon nanotubes: The practice of nanoscale process engineering. Chin Sci Bull, 2012, 57: 157–166
2 Tian L L, Zhuang Q C, Li J, et al. Mechanism of intercalation and deintercalation of lithium ions in graphene nanosheets. Chin Sci Bull, 2011, 56: 3204–3212
3 Chen M J, Yu F, Hu L J, et al. Recent progresses on the new condensed forms of single-walled carbon nanotubes and energy-harvesting devices. Chin Sci Bull, 2012, 57: 181–186
4 Ma Y W, Zhang L R, Li J J, et al. Carbon-nitrogen/graphene composite as metal-free electrocatalyst for the oxygen reduction reaction. Chin Sci Bull, 2011, 56: 3583–3589
5 Peng X, Zhou J, Wang W C, et al. Computer simulation for storage of methane and capture of carbon dioxide in carbon nanoscrolls by expansion of interlayer spacing. Carbon, 2010, 48: 3760–3768
6 Mpourmpakis G, Tylianakis E, Froudakis G E. Carbon nanoscrolls: Apromising material for hydrogen storage. Nano Lett, 2007, 7: 1893–1897
7 Shi X, Cheng Y, Pugno N M, et al. Molecular dynamics: Tunable water channels with carbon nanoscrolls. Small, 2010, 6: 739–744
8 Shi X, Cheng Y, Pugno N M, et al. A translational nanoactuator based on carbon nanoscrolls on substrates. Appl Phys Lett, 2010, 96: 053115
9 Bacon R. Growth, structure, and properties of graphite whiskers. J Appl Phys, 1960, 31: 283–290
10 Kaburagi Y, Hosoya K, Yoshida A, et al. Thin graphite skin on glass-like carbon fiber prepared at high temperature from cellulose fiber. Carbon, 2005, 43: 2817–2819
11 Viculis L M, Mack J J, Kaner R B. A chemical route to carbon nanoscrolls. Science, 2003, 299: 1361
12 Savoskin M V, Mochalin V N, Yaroshenko A P, et al. Carbon nanoscrolls produced from acceptor-type graphite intercalation compounds. Carbon, 2007, 45: 2797–2800
13 Shioyama H, Akita T. A new route to carbon nanotubes. Carbon, 2003, 41: 179–181
14 Xia D, Xue Q Z, Xie J, et al. Fabrication of carbon nanoscrolls from

monolayer graphene. Small, 2010, 6: 2010–2019
15 Patra N, Wang B, Kral P. Nanodroplet activated and guided folding of graphene nanostructures. Nano Lett, 2009, 9: 3766–3771
16 Stolyarova E, Stolyarov D, Bolotin K, et al. Observation of graphene bubbles and effective mass transport under graphene films. Nano Lett, 2009, 9: 332–337
17 Stoberl U, Wurstbauer U, Wegscheider W, et al. Morphology and flexibility of graphene and few-layer graphene on various substrates. Appl Phys Lett, 2008, 93: 051906
18 Gao Y, Chen X Q, Xu H, et al. Highly-efficient fabrication of nanoscrolls from functionalized graphene oxide by Langmuir-Blodgett method. Carbon, 2010, 48: 4475–4482
19 Zhang Z, Li T. Carbon nanotube initiated formation of carbon nanoscrolls. Appl Phys Lett, 2010, 97: 081909
20 Xie X, Ju L, Feng X F, et al. Controlled fabrication of high-quality carbon nanoscrolls from monolayer graphene. Nano Lett, 2009, 9: 2565–2570
21 Maple J R, Hwang M J, Stockfisch T P, et al. Derivation of class II force fields. I. Methodology and quantum force field for the alkyl functional group and alkane molecules. J Comput Chem, 1994, 15: 162–182
22 Sun H. Force field for computation of conformational energies, structures, and vibrational frequencies of aromatic polyesters. J Comput Chem, 1994, 15: 752–768
23 Sun H. Compass: An *ab initio* force-field optimized for condensed-phase applications overview with details on alkane and benzene compounds. J Phys Chem B, 1998, 102: 7338–7364
24 Sun H, Ren P, Fried J R. The COMPASS force field: Parameterization and validation for phosphazenes. Comput Theor Polym Sci, 1998, 8: 229–246
25 Rigby D, Sun H, Eichinger B E. Computer simulations of poly (ethylene oxide): Force field, PVT diagram and cyclization behaviour. Polym Int, 1997, 44: 311–330
26 Grujicic M, Cao G, Roy W N. Atomistic modeling of solubilization of carbon nanotubes by non-covalent functionalization with poly (*p*-phenylenevinylene-co-2,5-dioctoxy-*m*-phenylenevinylene). Appl Surf Sci, 2004, 227: 349–363
27 Xie J, Xue Q Z, Chen H J, et al. Influence of solid Surface and functional group on the collapse of carbon nanotubes. J Phys Chem C, 2010, 114: 2100–2107
28 Cote L J, Kim F, Huang J. Langmuir-Blodgett assembly of graphite oxide single layers. J Am Chem Soc, 2009, 131: 1043–1049
29 Szabo T, Hornok V, Schoonheydt R A, et al. Hybrid Langmuir-Blodgett monolayers of graphite oxide nanosheets. Carbon, 2010, 48: 1676–1680
30 Li X L, Liu Y Q, Fu L, et al. Synthesis and device integration of carbon nanotube/silica core-shell nanowires. J Phys Chem C, 2007, 111: 7661–7665
31 Guo Y B, Liu H B, Li Y J, et al. Controlled core-shell structure for efficiently enhancing field-emission properties of organic-inorganic hybrid nanorods. J Phys Chem C, 2009, 113: 12669–12673
32 Yi P, Poulikakos D, Walther J, et al. Molecular dynamics simulation of vaporization of an ultra-thin liquid argon layer on a surface. Int J Heat Mass Transfer, 2002, 45: 2087–2100